research articles Journal of proteome research

Systems Toxicology: Integrated Genomic, Proteomic and Metabonomic Analysis of Methapyrilene Induced Hepatotoxicity in the Rat

Andrew Craig,[†] James Sidaway,[‡] Elaine Holmes,[†] Terry Orton,[‡] David Jackson,[§] Rachel Rowlinson,[§] Janice Nickson,[§] Robert Tonge,[§] Ian Wilson,[||] and Jeremy Nicholson*,[†]

Biological Chemistry, Biomedical Sciences Division, Faculty of Life Sciences, Imperial College London, Sir Alexander Fleming Building, South Kensington, London SW7 2AZ, United Kingdom, Safety Assessment, AstraZeneca, Alderley Park, Macclesfield, Cheshire SK104 TG, United Kingdom, Pathways, Discovery Enabling Capabilities and Sciences, AstraZeneca, Alderley Park, Macclesfield, Cheshire SK10 4TG, United Kingdom, and Department of Drug Metabolism and Pharmacokinetics, AstraZeneca, Alderley Park, Macclesfield, Cheshire SK104TG, United Kingdom

Received October 5, 2005

Administration of high doses of the histamine antagonist methapyrilene to rats causes periportal liver necrosis. The mechanism of toxicity is ill-defined and here we have utilized an integrated systems approach to understanding the toxic mechanisms by combining proteomics, metabonomics by ^{1}H NMR spectroscopy and genomics by microarray gene expression profiling. Male rats were dosed with methapyrilene for 3 days at 150 mg/kg/day, which was sufficient to induce liver necrosis, or a subtoxic dose of 50 mg/kg/day. Urine was collected over 24 h each day, while blood and liver tissues were obtained at 2 h after the final dose. The resulting data further define the changes that occur in signal transduction and metabolic pathways during methapyrilene hepatotoxicity, revealing modification of expression levels of genes and proteins associated with oxidative stress and a change in energy usage that is reflected in both gene/protein expression patterns and metabolites. The difficulties of combining and interpreting multiomic data are considered.

Keywords: genomics • microarray • proteomics • metabonomics • hepatotoxicity • methapyrilene

1. Introduction

Understanding the etiology and mechanisms of human disease is a major goal of 21st century medical research. This has led to the development of molecular systems biology, which is concerned with unraveling the integrated functioning of biological systems in terms of the structure and dynamics of networks of biomolecules as well as capturing these characteristics in silico in order to derive fundamental insight into holistic biological function. Recent analytical developments have made feasible the global assessment of levels of entire classes of biomolecules at a rate of sample throughput facilitating extensive experimental design. These omic approaches include microarrays, to assess global gene expression patterns (part of the field of genomics), high-resolution fluorescence two-dimensional gel electrophoresis and mass spectrometry to quantify and identify holistic protein changes (proteomics) and ^{1}H NMR spectroscopy to measure multiple metabolites (metabonomics). Hitherto such 'omics' methods have generally been used independently to investigate disruption of complex systems[1−4] with the common rationale that measuring large numbers of parameters coupled to statistical analysis might reveal patterns of regulation within these networks. Such patterns should be related quantitatively to changes in established biological endpoints. Therefore, it follows that in order to approach a systems level description of an organism these parallel 'omics' technologies should begin to be integrated and that the result of this integration might be expected to be highly synergistic. To date only a few reports of this sort of approach exist, and these include a study of hydrazine toxicity in the rat[5] as well as two investigations of APAP toxicity.[6,7]

In the field of toxicology, there is ample opportunity to design experiments that utilize omic approaches singly or in parallel to investigate toxic mechanisms. Two recent reports have described the application of microarray technology to investigate global liver gene expression profiles in response to methapyrilene [*N*-dimethyl-*N*′-pyridyl-*N*′(2-thienylmethyl)-1,2-ethanediamine] toxicity in the rat.[8,9] Both studies used methapyrilene as an exemplar hepatotoxin and successfully demonstrated a strong correlation between changes in histopathologic damage and gene expression changes. Gene expression pathways were identified which relate to methapyrilene toxicity after 24 h[8] or 7 days.[9] There have also been a number of

* To whom correspondence should be addressed. E-mail: j.nicholson@imperial.ac.uk.
[†] Imperial College London.
[‡] Safety assessment, AstraZeneca.
[§] Discovery Enabling Capabilities and Sciences, AstraZeneca.
[||] Department of Drug Metabolism and Pharmacokinetics, AstraZeneca.

10.1021/pr0503376 CCC: $33.50
Published on Web 06/15/2006

proteomic investigations on methapyrilene hepatotoxicity,[10−12] but as far as protein identification is concerned, advances over the early findings[10] have been few. The fundamental observations being evidence of covalent modifications of rat mitochondrial matrix and inner membrane proteins, together with protein abundance changes in other organelle fractions. Four of these proteins (mitochondrial F1 ATPase β-subunit, heat shock protein 58, glucose regulated protein 75 and carbamoyl phosphate synthase) were identified by comparison to reference 2D gel maps, but no information was given on the vast majority of affected proteins.

Acute high dose administration of a variety of chemical classes in experimental animals and man may result in hepatotoxicity. One common toxic mechanism is via the cytochrome P450 (CYP) mediated generation of reactive metabolites, as exemplified by acetaminophen (APAP) hepatotoxicity. In the case of APAP, it is a CYP-generated reactive metabolite that is thought to covalently bind to proteins causing mitochondrial dysfunction which in turn induces oxidative stress followed by cell death.[13] The majority of hepatotoxins (including APAP) induce centrilobular necrosis, which is associated with the highest level of CYP expression.[14] Less commonly certain hepatotoxins such as allyl alcohol cause necrosis in the periportal portion of the liver lobule.[15] Methapyrilene is another agent where administration to rats causes periportal necrosis, associated with inflammation and bile duct hyperplasia.[16] Despite the several omic investigations described above, the mechanism of methapyrilene hepatotoxicity is still adumbrate, although there are certain similarities to acetaminophen (APAP) hepatotoxicity. In vivo studies in rats and in isolated hepatocytes suggested that biotransformation by a specific CYP isoform, CYP2C11, result in the formation of a reactive metabolite.[17,18] Biliary excretion of metabolites of methapyrilene could also be important as interruption of enterohepatic circulation abrogated the toxicity.[19] Two glucuronide conjugates of methapyrilene were also found in bile, however it is unclear how, if at all, they relate to the formation of a reactive metabolite. In rats methapyrilene induces liver mitochondrial proliferation[20] and promotes covalent modification of proteins within the organelle[21] which might be associated with the drug or a metabolite.[22] In isolated rat hepatocytes, inhibition of mitochondrial transition permeability pore opening and prevention of intracellular Ca^{2+} mobilization reduced methapyrilene toxicity, strongly implicates loss of mitochondrial Ca^{2+} homeostasis in the toxic mechanism.[18] Although methapyrilene caused depletion of glutathione in isolated rat hepatocytes suggesting oxidative stress,[17] no depletion in glutathione or glutathione-related enzymes was observed in intact rats.[19]

Here, we have used a combination of microarray gene expression profiling, proteomics and metabonomics to study the effects of the daily administration of methapyrilene at 50 and 150 mg/kg for 3 days to male rats. The lower dose of the drug is approximately 10% of the rat LD50 value while the desired toxicity at the high dose has been previously reported.[19] Our aim was to determine the impact of drug toxicity on hepatic metabolic pathways and also ascertain whether a multiomic systems biology approach would result in improved understanding of the mechanism of hepatotoxicity of the drug. This study serves to demonstrate one approach to the experimental arm of an integrated multiomic systems biology strategy and forms a platform upon which to develop the necessary computational methodologies. It will be necessary to produce extremely well characterized models in order to ensure robust modeling approaches are developed which maximize the recovery of latent information from the multiple parallel data sets and deliver real predictive value.

2. Materials and Methods

2.1. Materials. Unless otherwise stated, all materials were obtained from Sigma-Aldrich Ltd (Poole, UK).

2.2. Animals and Dosing. All animal studies were conducted under UK Home Office License according to appropriate legislation. Male Wistar derived Alp*K*:AP$_f$SD (Alderley Park) rats of between 170 and 200 g body weight were obtained from the Rodent Breeding Unit at AstraZeneca Alderley Park. The rats were housed in metabolism cages and subjected to 12-h light, 12-h dark artificial light cycle with food (standard rat and mouse diet Number 1 modified irradiated diet; Special Diet Services, Witham Essex UK) and water available ad libitum. Environmental conditions such as temperature and humidity were controlled and the animals were acclimatized to these conditions for 3 days prior to commencement of dosing. The rats were divided into three groups of five and dosed by gavage with water (vehicle), 50 mg/kg/day methapyrilene (Sigma-Aldrich) or 150 mg/kg/day methapyrilene. After 3 days of dosing the rats were euthanased by CO_2 inhalation 2 h after the final dose.

2.3. Sample Collection. Urine from animals in metabolism cages was collected onto dry ice (0−26, 26−50, 50−74 h after administration of the first dose). Urine samples were stored at −40 °C pending analysis via NMR spectroscopy. Blood samples were withdrawn by cardiac puncture immediately post euthanasia and placed in EDTA coated tubes from which plasma samples were isolated by centrifugation for blood chemistry analysis. The livers were removed immediately after sacrifice, weighed, and then cut into small pieces. A small portion of each liver approximately 0.1 mg from the left lateral lobe was homogenized in 10 mL of guanidine thiocyanate buffer (guanidium thiocyanate 4 M, sodium citrate 25 mM, sarcosyl 0.5%, 2-mercaptoethanol 0.1 M) to prevent degradation of the RNA. A section of intact liver was also taken from the left lateral lobe for histology. The remaining portions of liver were snap frozen in liquid nitrogen and stored at −80 °C until required for proteomic or metabonomic analysis. In all cases tissue from the left lateral lobe was used in order to standardize the analysis across 'omics' platforms as far as possible.

2.4. Histology and Liver Enzyme Measurement. A small sample of the four major liver lobes (left and right lateral, left and right medial lobes) was taken and preserved in neutral buffered formalin. One histological section from the left lateral lobe was prepared from each sample, stained with H and E, and examined by light microscopy. Serum levels of alanine aminotransferase (ALT), aspartate aminotransferase (AST) and L-glutamate dehydrogenase (GLDH) were quantified using colorimetric assays.

2.5. Gene Expression Analysis. RNA was isolated from frozen liver samples with Qiagen RNeasy mini kits (Qiagen Ltd., West Sussex, UK), according to the manufacturers protocol. RNA integrity was also confirmed by agarose gel electrophoresis. Gene expression data were generated using the Rat Genome U34A gene chip (Affymetrix, High Wycombe, UK) from three individual animals per group. Total RNA (10 μg) was labeled and processed according to the manufacturer's instructions. Microarray Suite 5 (Affymetrix) was used to perform the image digitization, quantification, and probe set summarization of the microarray data. The microarray data were normalized using

robust regression. A gene was considered to have changed if it was regulated at least 2-fold (up or down) relative to the control group and the difference was statistically significant ($P < 0.05$ by unpaired student's t test). For all up regulated genes the probe set had to be called 'present' by the Affymetrix 'absolute call' metric in all samples within the treated group; for all down regulated genes the probe set had to be called 'present' in all control samples. For each probe set, the corresponding gene was identified using the NetAffx database (Affymetrix) and the associated Gene Ontology information was used for assigning to particular metabolic and functional pathways.

2.6. Proteomics. 2.6.1. Proteomics Suppliers. Cy3, Cy5 (all lysine labeling chemistries), Pharmalytes pH 3−10, DryStrip Cover Fluid, Hybond C Super nitrocellulose membrane, Sodium dodecyl sulfate (SDS) and Immobilized pH Gradient (IPG) Immobiline DryStrips (pH 3−10NL 24 cm) were from GE Healthcare (Amersham, UK). Stock acrylamide solution was supplied as Protogel (ultrapure protein sequencing and electrophoresis grade, gas stabilized, 30% w/v acrylamide, 0.8% w/v bis-acrylamide: National Diagnostics, Hull, UK). Trypsin (sequence grade) was from Boehringer Mannheim (Lewes, UK). α-Cyano-4-hydroxycinnamic acid and dimethylformamide (DMF) were from Aldrich (Dorset, UK). α-Cyano-4-hydroxycinnamic acid was recrystallized and matrix solution was made up as a 10 mg/mL solution in 0.1% v/v TFA/ 60% v/v acetonitrile. Antipain, leupeptin, aprotinin, phenylmethylsulfonyl fluoride (PMSF), bovine serum albumin (BSA), 3-[(3-Cholamidopropyl)dimethylammonio]-1-propanesulfonate hydrate (CHAPS), lysine, Sucrose, Coomassie Brilliant Blue G-250, PAGBond film, Tris base, dithiothreitol (DTT) and iodoacetamide (IAA) were from Sigma (Dorset, UK). Urea (ultrapure) was from ICN Biomedicals (Aurora, USA). Bromophenol blue was from Bio-Rad (Hemel Hempstead, UK). Trifluoroacetate (TFA) and acetonitrile (sequencing grade) were from PE Biosystems (Warrington, UK). EDTA, glycerol and thiourea were from Fisher (Loughborough, UK).

2.6.2. Samples for Proteomic Analysis. Samples from each individual rat were pooled within a treatment group and each pool was labeled with Cy3 and run on individual gels in triplicate. Every gel was also comigrated with a Cy5 standard comprising all three sample pools mixed together to form a 'super-pool' internal standard. Five samples were pooled to make up the control and 50 mg/kg/day methapyrilene groups and four samples made up the 150 mg/kg/group. In turn, nine gels would be formed by triplicate repeats of each group. These provided the control, low (pharmacological but nontoxic) and high (toxic) dose groups.

2.6.3. Proteomics Sample Processing. Individual rat livers were homogenized separately into 5−10 mL homogenization buffer (10 mM Tris-HCl (pH 7.4), 0.25 M sucrose, 1 mM EDTA, 0.5 g/L BSA, 2.5 mg/L aprotinin, antipain and leupeptin, and 1 mM PMSF) using a Potter-type homogenizer (Fisher Scientific, Loughborough, UK) (10 strokes). Unbroken cells and connective tissue were removed from the homogenates by centrifugation (250 × *g* for 10 min). The supernatants were stored at −80 °C. Protein content was assayed by a modified Bradford assay against BSA in a background of the lysis buffer (omitting the protease inhibitors).

2.7. Proteomics 2D-Difference Gel Electrophoresis (DIGE) Dye Labeling. 2D-DIGE was carried out essentially as described by Tonge et al.[23] Liver samples were diluted to 3 mg/mL in 2D-DIGE labeling buffer containing a protease inhibitor (7 M urea, 2 M thiourea, 4% w/v CHAPS, 1 mM Pefabloc SC inhibitor and protector reagent). Samples were solubilized by shaking on a rotary table mixer for 1 h followed by a 5 min centrifugation at 14 000 rpm (Eppendorf centrifuge 5415C, rotor radius 65 mm). Supernatants were pooled, as appropriate, by equal protein amount and mixed for 3 min prior to labeling. The pH of the sample was adjusted to 8.5 for labeling by addition of 1 M Tris-HCl, pH 9.5 to give a final composition of 50 mM Tris. Samples were labeled on ice with Cy3 or Cy5 (stock diluted 1 in 5 in fresh dry DMF). Labeling was in the ratio 200 pmol dye: 50 μg protein and was for 30 min. The reaction was quenched by addition of 1 μL of 10mM lysine per 200 pmol dye used, for 10 min on ice. IEF buffer was then added with double the desired concentration of DTT and pharmalytes to achieve the final IEF rehydration solution composition (as above for DIGE labeling buffer, less the inhibitor, containing 60 mM DTT (0.93% w/v) and 0.2% v/v pharmalytes pH 3−10). This was allowed to mix for 15 min at room temperature. Samples were then frozen at −80 °C until application onto IPG strips. All labeling steps were carried out protected from light and samples were mixed briefly and pulsed in a microcentrifuge between steps.

2.7.1. Proteomics Isoelectric Focusing (IEF). A 100-μg portion of each Cy3 and Cy5 sample were added together and adjusted to 250 μL IPG strip re-hydration volume. The final composition was 7 M urea, 2 M thiourea, 4% w/v CHAPS, 30 mM DTT (0.46% w/v), and 0.2% w/v Pharmalytes pH 3−10) with a trace of bromophenol blue. The solution was mixed on a rotary table mixer for 1 h, and centrifuged at 14 000 rpm for 5 min. The supernatant was loaded onto 24 cm pH 3−10 NL IPG strips and re-hydrated overnight. While the initial solution was re-hydrating the IPG strip, 200 μL further re-hydration buffer was added to the pellet and mixed for a further 2 h. At that point, the tubes were again centrifuged, and the remaining fluid applied to the IPG strip. Re-hydration overnight was followed by isoelectric focusing in a rising-step voltage protocol for 110 kVh (20 °C, 10 mA). IEF was achieved using the Multiphor II unit (GE Healthcare). Strips were then frozen at −80 °C until application onto 2D gels. All IEF steps were carried out protected from light.

2.8. Proteomics SDS-Polyacrylamide Gel Electrophoresis (SDS-PAGE) and Image Capture. IPG Strips were equilibrated in a two-step protocol in pH 6.8 equilibration buffer (100 mM Tris, 6 M Urea, 30% v/v glycerol, 1% w/v SDS) containing 1% w/v DTT for 15 min, followed by 4% w/v IAA for 15 min, and applied to vertical 10% w/v SDS-PAGE gels for the second dimension separation using a modified ESA investigator gel system (Genomic Solutions, Ann Arbor, MI). A bromophenol blue dyefront was used to monitor electrophoresis and gels were removed from the tanks upon migration of the dyefront from the gel. The resulting gels were scanned using a Typhoon 9400 scanner (GE Healthcare) and saved as .gel files for analysis. Scan settings were optimized to obtain a maximum signal of approximately 80 000 counts (of 100 000) per channel. Optimal photomultiplier tube (PMT) voltage settings on the typhoon used were 530V for Cy3 and 485V for Cy5. Final scans were at 100 μm resolution.

2.8.1. Proteomics Image Analysis. Gel images were analyzed using Progenesis (V.2004) with the CSA cross-stain analysis module (Non Linear Dynamics, UK). Cropped images were loaded for each gel. Images were grouped by gel (Cy3-Cy5 group from a single gel) and then gels were matched to allow comparison of average gels between groups. Each average gel was composed of triplicates of the same pooled sample;

therefore triplication was to address any experimental variation and did not represent biological replicates. Spots were required to be present and matched in all three members of a class to be represented in average gel calculations, and a minimum spot area of 100 units was set. Otherwise, parameters were as default. Detection and matching were inspected and corrected where necessary. The groups were then compared using the pairwise filtering tool in the software. Spots altered by 2-fold in terms of average normalized volume between groups and with a t-test P value ≤ 0.05 were selected. The low and high dose groups were compared to the control group in turn and conserved changes were also noted.

2.8.2. Proteomics Protein Identification by Mass Spectrometry. Preparatory gels were run using the same IEF protocol as above. The sample with the highest protein concentration was used to represent the group. 0.5 mg protein was loaded for silver stained gels, and 0.75 mg for Coomassie stained gels. This required six gels, one for each animal group by each staining method (3×2). Visualization by colloidal Coomassie and silver staining used protocols modified from the literature.[24−26] Gels were scanned using the ImageScanner (GE Healthcare) to generate 8-bit images. Adhesive reference markers (GE Healthcare) were attached to the backing film prior to scanning for triangulation purposes. Gel images were loaded into a Progenesis single-stain workspace and spots for excision added to the images manually with a spot size corresponding to a 2 mm diameter circular cut on the gel surface. These were then imported to the analytical experiment and matched to the reference gel for records. Pick lists were prepared and exported for excision of spots. Spots were excised using the Ettan SpotPicker (GE Healthcare) and stored at −20 °C until MS analysis.

Protein spots of interest from 2D polyacrylamide gels were digested and peptides extracted as described previously (23). Peptide masses were measured over m/z range 850−3500 using a MALDI delayed extraction reflectron time-of-flight mass spectrometer (Voyager DE-STR, Applied Biosystems,UK) equipped with a nitrogen laser (337 nm). Peptides were cocrystallized with an equal volume of 5 mg/mL alpha-cyano-4-hdroxycinamic acid in 60% ACN, 0.1% TFA. The MALDI spectra were calibrated using external calibration very close (ca. 1 mm) to the actual spots; this normally provided mass accuracy of approximately 50−100 ppm. The resultant peptide fingerprints were searched against a mammalian subset of an in-house nonredundant protein database (AA_hmr) using the Mascot search engine (www.matrixscience.com). If the fingerprints failed to yield confident protein hits or if the spectra contained a significant number of unmatched peaks, follow up LC−MS/MS (by on-line or off-line methods) was carried out on these samples.

The on-line LC−MS/MS method used an Ultimate nano-LC system (Dionex, UK) linked directly via a nanoflow probe to a Q-TOF1 (Waters, UK). Samples were separated by reversed-phase nano-LC using a 15 cm × 75 μm ID Pepmap column (LC Packings) at a flow rate of 300 nL/min, Buffer A − 0.1% formic acid, Buffer B − 0.1% formic acid, 95% ACN. A separation gradient was used (0 min 5% B, 31 min 57%B followed by a 90% B wash and reequilibration to 5%B). The system was run in positive ion mode with automated data dependent MS to MS/MS switching on the 4 most intense ions of charge states 2+ to 4+ detected in the survey scan over m/z range of 350 to 1600 Da. MS/MS data were collected using 1 s scans over m/z range 50−2000 Da with external calibration. The resultant combined MS and MS/MS data files were searched as above using the Mascot search engine.

If unmatched peaks not consistent with the identity proposed were present, the observed peaks could match several proteins, or no clear identity was obtained, the sample was analyzed by MS/MS QTOF (Micromass, UK). Data were collected from m/z 50−2000. MS/MS spectra were searched against Mascot Daemon and also manually interpreted to derive sequence information of at least six consecutive amino acids. These were searched against a mammalian subset of the Swiss-Prot/TrEMBL databases, and proprietary databases. Reported hits were confirmed by further examination of tryptic peptides predicted by the identity. Further contributing factors were whether both techniques identified the same protein, the expected mass and pI of the protein from the gel, and user assessment of the quality and amount of sequence data.

2.9. ^{1}H NMR Spectroscopy of Urine. For analysis, a 600 μL aliquot of urine was mixed with 400 μL of phosphate buffer solution (composition below) in a microfuge tube. This mixture was centrifuged in a benchtop centrifuge at 13 000 rpm for 10 minutes (Eppendorf centrifuge 5415C, rotor radius 65 mm) in order to spin down particulates. The resulting liquid was then decanted into sample vials compatible with the Bruker Efficient Sample Transfer (BEST) system (Bruker Biospin Rheinstetten Germany). The samples were stored overnight at 4 °C prior to analysis by ^{1}H NMR. Buffer solution (0.02 M with respect to phosphate) was prepared at pH 7.4 in 80:20 H_2O:D_2O (V/V) (28.85 g Na_2HPO_4, 5.25 g NaH_2PO_4, 172 mg protonated sodium trimethylsilyl [2,2,3,3-H_4] propionate (TSP) 1 mM, 190 mg sodium azide in 1 L). TSP was included as an internal chemical shift standard (0.00 ppm) and D_2O as a spectrometer frequency lock. Sodium azide was to prevent bacterial growth and changes in sample composition over the course of the experiment.

All ^{1}H NMR spectra were acquired on a Bruker DRX600 ultrashielded spectrometer at a proton observation frequency of 600.13 MHz and at room temperature with a flow injection system (BEST) and a 4 mm (120 μL) flow injection probe. A standard 1D pulse sequence using the first increment of the noesy pulse sequence was used in order to achieve suppression of water signals with selective irradiation of the water resonance for a period of 1 s during the relaxation delay before the first pulse and during the 150 ms mixing time. For each sample 128 transients were acquired into 32k data points with a spectral width of 20.036 ppm. An exponential weighting function was applied to each transient prior to Fourier transformation corresponding to a line broadening of 1 Hz.

2.10. ^{1}H MAS NMR Spectroscopy of Intact Liver Tissue. For each animal, a small piece of frozen liver was placed into a watch glass and whetted with several drops of D_2O from a Pasteur pipet. The liver piece was then trimmed using a scalpel to yield a cube approximately 16 μL in volume from the center of the original sample. Care was taken at this point to take tissue from within the liver so as to minimize inclusion of the fatty covering of the liver surface. Samples were placed in 4 mm outer diameter zirconium oxide rotors and rotated at 5 kHz.

Spectra were acquired on a Bruker DRX600 ultrashielded spectrometer at a proton observation frequency of 600.13 MHz with an MAS probe and at room temperature. A standard one-dimensional NMR spectrum was obtained using the noesypr1d pulse sequence (first increment of the noesy pulse sequence) in order to achieve suppression of water signals. For each sample 256 transients were acquired into 32k data points with

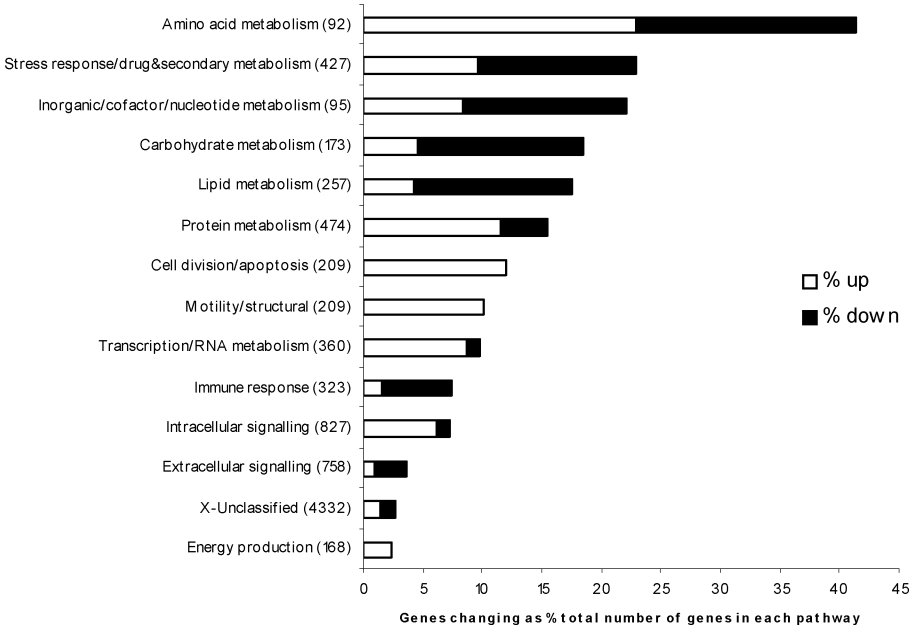

Figure 1. Genes changing as a percentage of each pathway. Numbers in brackets refer to the total number of probe sets on the Affymetrix rat genome U34A chip allocated to each metabolic/functional pathway. The number of probe sets that were considered to have changed either up or down in response to 150 mg/kg methapyrilene treatment were expressed as a percentage of the total for each pathway.

a spectral width of 20.036 ppm. An exponential weighting function was applied to each transient prior to Fourier transformation corresponding to a line broadening of 1 Hz.

2.11. Spectral Data Processing and Analysis. All spectra were phase and baseline corrected using an in house automatic routine written by Dr TMD Ebbels and Dr HC Keun in the Matlab language (The MathWorks, Natick, Massachusetts). Urine spectra were automatically referenced to the TSP signal while tissue spectra were manually referenced to the signal from the anomeric proton at δ 5.233 of α-glucose. Metabolites were identified by reference to chemical shift tables and further 2-dimensional NMR experiments where necessary.

At this point, each tissue NMR spectrum was simplified to 900 variables, calculated by integrating regions of equal width (0.01 ppm) over the δ range 0.5−10 using Matlab and code written by Dr Olivier Cloarec. The regions δ 4.50−5.98, were eliminated to remove any spurious effects of variability in the efficiency of water suppression and any modulation of other signals in this region due to cross relaxation effects via proton exchange. The reduced spectral datasets were then normalized to take into account gross variations in sample composition due to urine "concentration" or tissue mass. The total integral of each spectrum was set to a value of 100. Analysis of spectral data by OPLS[27] in discriminant analysis mode was performed using in house software written by Dr Olivier Cloarec.[28]

3. Results

3.1. Histology and Liver Enzymes. Liver tissues were examined by microscopy in order to confirm the type and extent of the liver lesion. Mild to moderate periportal hepatocyte degeneration and necrosis occurred in all five animals receiving 150 mg/kg/day methapyrilene (HD) after 3 days. These findings were less severe in the 50 mg/kg/day dose (LD) group and were only observed in two out of five rats. The control animals displayed no sign of periportal hepatocyte degeneration or necrosis. Additionally, periportal acute inflammatory cell infiltration was observed exclusively in animals receiving the high dose methapyrilene treatment; this was not observed in the control or lower dose groups. These histological findings were accompanied by combined elevation of plasma transaminases and GLDH in high dose animals (mean ± SE U/L [ALT Ctrl 62.2 ± 18.1, LD 56.2 ± 10.8, HD 222.7 ± 115] [AST Ctrl 111.8 ± 28.4, LD 132 ± 26.9, HD 632 ± 329] [GLDH Ctrl 12.2 ± 6.5, LD 50 ± 2.3, HD 280 ± 140.6]).

3.2. Liver Gene Expression Changes. When Affymetrix gene expression analysis was carried out on the livers of animals dosed with methapyrilene 351 probe sets were identified out of the 8799 present on the RGU134A chip, which were upregulated (at least 2-fold relative to the control group ($P < 0.05$)) as a result of methapyrilene exposure for 3 days at either 50 mg/kg or 150 mg/kg while a further 268 probe sets were down regulated. The number of probe sets modulated increased substantially as a result of toxicity as only 52 probe sets were altered in the 50 mg/kg group, whereas 606 probe sets changed in the 150 mg/kg group alone. A total of 39 changes in the probe sets were common to both groups.

The probe sets regulated by methapyrilene were assigned to genes and metabolic/functional pathways using public domain annotation. The proportion of genes with expression changing in each metabolic/functional pathway is shown in Figure 1. All types of pathway were affected to some degree by methapyrilene exposure. Representative gene changes that are associated with these pathways are described in Tables 1−3 (full gene list is available in supplementary data). Genes encoding proteins involved in metabolic pathways such as amino acid metabolism were among those most strongly altered (Figure 1) and included enzymes involved in taurine and tryptophan metabolism and the urea cycle (Table 1). Lipid metabolism, protein metabolism and carbohydrate metabolism (Table 1) were also altered, and included enzymes involved in glycolysis/gluconeogenesis, fatty acid oxidation/synthesis, sterol synthesis and retinoid/bile acid metabolism. In a small

Table 1. Representative Gene Expression Changes Associated with Energy Production and Amino Acid, Protein, Glucose, and Lipid Metabolism[a]

Probeset	Gene Title	Pathway	Vehicle Signal value	Methap 50mkd FC	Methap 150mkd FC
M64755_at	cysteine-sulfinate decarboxylase	Amino acid metabolism	1459	-2.2	-3.7*
rc_AA942685_at	cytosolic cysteine dioxygenase 1	Amino acid metabolism	5133	-1.2	-2.6**
U68168_at	kynureninase (L-kynurenine hydrolase)	Amino acid metabolism	2375	-2.4*	-5.6***
Z50144_g_at	kynurenine aminotransferase 2	Amino acid metabolism	536	-1.6	-3.4***
D13978_s_at	argininosuccinate lyase	Amino acid metabolism	914	2.6*	2.7**
J04792_at	ornithine decarboxylase 1	Amino acid metabolism	151	2.5	4.9***
M11266_at	ornithine transcarbamylase	Amino acid metabolism	1951	-1.5	-2.6***
AF080468_g_at	glucose-6-phosphatase, transport protein 1	Carbohydrate metabolism	1738	-1.4	-3.8*
L01793_g_at	glycogenin	Carbohydrate metabolism	48	1.1	2.2*
X04069_at	liver glycogen phosphorylase	Carbohydrate metabolism	363	-3.3*	-2.3**
rc_AI012595_at	protein phosphatase 2a, catalytic subunit, alpha isoform	Carbohydrate metabolism	508	1.3	2.9*
M83298_at	protein phosphatase 2a, regulatory subunit B, alpha isoform	Carbohydrate metabolism	51	1.6*	2.8**
M12919mRNA#2_a	aldolase A	Carbohydrate metabolism	241	2.2	4.1*
rc_AA892395_s_at	aldolase B	Carbohydrate metabolism	6326	-1.4	-3***
M86240_at	fructose-1,6- biphosphatase 1	Carbohydrate metabolism	4656	-1.4	-2.8*
X53588_at	glucokinase	Carbohydrate metabolism	557	1.1	-5.2**
rc_AA945442_at	glucokinase regulatory protein	Carbohydrate metabolism	996	-2.3*	-3.7***
L37333_s_at	glucose-6-phosphatase, catalytic	Carbohydrate metabolism	1722	-2.6	-6.7***
U32314_at	pyruvate carboxylase	Carbohydrate metabolism	775	-2.5**	-4.6***
X05684_at	pyruvate kinase, liver and RBC	Carbohydrate metabolism	263	-3.1*	-7*
rc_AI171506_g_at	malic enzyme 1	Carbohydrate metabolism	625	-2.5*	-1.6
L22294_at	pyruvate dehydrogenase kinase 1	Carbohydrate metabolism	174	-1.5	-2.2*
U10357_g_at	pyruvate dehydrogenase kinase 2	Carbohydrate metabolism	712	-1.4	-2.1*
D13122_f_at	ATPase inhibitor	Energy production	157	1.8**	3.9*
rc_AI232307_at	Cox7a2l protein (LOC298762), mRNA	Energy production	361	1.3	2.3**
D12770_s_at	solute carrier family 25 member 4	Energy production	78	1.1	2.6**
M22360_s_at	alpha(1)-inhibitor 3, variant I	Protein metabolism	2622	-2.8	-4.7**
X07648cds_at	amyloid beta (A4) precursor protein	Protein metabolism	269	1.8	4.3*
U38253_g_at	eukaryotic translation initiation factor 2B, subunit 3	Protein metabolism	36	1.9	4.5**
U05014_g_at	eukaryotic translation initiation factor 4E binding protein 1	Protein metabolism	291	2*	3.9**
rc_AA858673_at	pancreatic secretory trypsin inhibitor type II (PSTI-II)	Protein metabolism	2959	-1.6*	-10***
rc_AA892298_at	peptidylprolyl isomerase (cyclophilin)-like 3	Protein metabolism	18	2.3	4*
X58465mRNA_at	ribosomal protein S5	Protein metabolism	618	1.8	3.6***
X95189_at	acyl-Coenzyme A oxidase 2, branched chain	Lipid metabolism	1268	-1.2	-2.2***
rc_AI170568_s_at	dodecenoyl-coenzyme A delta isomerase	Lipid metabolism	593	3.2	3.2*
D90109_at	fatty acid Coenzyme A ligase, long chain 2	Lipid metabolism	1995	-1.5	-3.3**
AB012933_at	fatty acid Coenzyme A ligase, long chain 5	Lipid metabolism	942	-2.1*	-2.1***
J05210_at	ATP citrate lyase	Lipid metabolism	1305	-2.4*	-3.2*
X13527cds_s_at	fatty acid synthase	Lipid metabolism	690	-1.8	-2.7***
rc_AI237731_s_at	lipoprotein lipase	Lipid metabolism	42	1.8	2.4*
X95577_at	protein kinase, AMP-activated, beta 1 non-catalytic subunit	Lipid metabolism	277	-1.4	-2.7**
rc_AI175764_s_at	stearoyl-Coenzyme A desaturase 1	Lipid metabolism	634	-5.1*	-9.7**
AF036761_g_at	stearoyl-Coenzyme A desaturase 2	Lipid metabolism	1307	-6.9**	-16.7***
L32601_s_at	20 alpha-hydroxysteroid dehydrogenase	Lipid metabolism	185	1.2	-2.7**
rc_AA817846_at	3-hydroxybutyrate dehydrogenase (heart, mitochondrial)	Lipid metabolism	1510	-2*	-3.3***
rc_AA892832_at	fatty acid elongase 1	Lipid metabolism	4490	-2.1	-4.2**
M67465_at	hydroxy-delta-5-steroid dehydrogenase	Lipid metabolism	1045	-2.3	-5.1**
rc_AI105448_at	hydroxysteroid 11-beta dehydrogenase 1	Lipid metabolism	5636	-1.6*	-2.7**
Y09333_at	mitochondrial acyl-CoA thioesterase 1	Lipid metabolism	90	7.1	13.2*
J05035_g_at	steroid 5 alpha-reductase 1	Lipid metabolism	2137	-1.5	-7.9**
M00002_at	apolipoprotein A-IV	Lipid metabolism	1263	-2.5*	-2.5*
J02596cds_g_at	apolipoprotein C-III	Lipid metabolism	9327	-1.4*	-2.7**
V01235_at	fatty acid binding protein 1	Lipid metabolism	6772	-1.7	-3.2**
U02096_at	fatty acid binding protein 7	Lipid metabolism	472	-1.5	-4.2*
M16235_at	lipase, hepatic	Lipid metabolism	1553	-1.6	-3.1**
D45252_s_at	2,3-oxidosqualene: lanosterol cyclase	Lipid metabolism	269	-2.5*	-2.1*
X55286_g_at	3-hydroxy-3-methylglutaryl-Coenzyme A reductase	Lipid metabolism	85	1.3	3*
X52625_at	3-hydroxy-3-methylglutaryl-Coenzyme A synthase 1	Lipid metabolism	2741	-1.8	-2.2*
L16995_at	sterol regulatory element binding factor 1	Lipid metabolism	342	-1.4**	-2.1**
M58287_s_at	sterol carrier protein 2	Lipid metabolism	100	-1.5	-2.1*
AF001898_at	aldehyde dehydrogenase family 1, member A1	Lipid metabolism	710	2.1	4.5*
M19257_at	retinol binding protein 1	Lipid metabolism	1378	-2.1***	-2.8**
U33500_g_at	retinol dehydrogenase type II (RODH II)	Lipid metabolism	452	-1.2	-2.1*
U18762_at	retinol dehydrogenase type III	Lipid metabolism	287	-1.8*	-4.4***
U89905_at	alpha-methylacyl-CoA racemase	Lipid metabolism	908	-1.5	-2.7**
D86086_s_at	ATP-binding cassette, sub-family C (CFTR/MRP), member 2	Lipid metabolism	712	1.3	2.9*
D43964_at	bile acid-Coenzyme A: amino acid N-acyltransferase	Lipid metabolism	2486	-1.6	-2.4**

[a] Gene expression changes are expressed as a fold change (FC) relative to the mean vehicle signal value, * = $P < 0.05$, ** = $P < 0.01$, *** = $P < 0.001$, mkd = mg/kg/day.

number of cases, the response observed at low dose was reversed at the high dose. For example, UDP glycosyltransferase1 family polypeptide A2 was found to be slightly reduced in the low dose group while a marked increase in the expression was noted at high dose. Further experiments are warranted to further explore this altered behavior in gene expression.

Another metabolic/functional pathway significantly modulated by methapyrilene consisted of proteins involved in the antioxidant stress response and drug metabolism, such as glutathione metabolism, stress response, P450 metabolism, and Phase II metabolism (Figure 1, Table 2). These included enzymes previously implicated in mechanism of methapyrilene toxicity such as the CYP2C family and UDP glycosyltransferases (glucuronidation). Notable in this group was the large induction of the multidrug resistance *P*-glycoprotein.

In contrast to the other pathways, only upregulated genes were observed in the cell division/apoptosis and the motility/structural pathways, with a predominance of upregulated genes

Table 2. Representative Gene Expression Changes Associated with the Stress Response and Drug, Secondary and Co-factor Metabolism[a]

Probeset	Gene Title	Pathway	Vehicle Signal value	Methap 50mkd FC	Methap 150mkd FC
E01184cds_s_at	cytochrome P450 1A1	Drug & secondary metabolism	1571	-1.2	-6.2***
M26127_s_at	cytochrome P450 1A2	Drug & secondary metabolism	1651	-1.2	-4.9***
J04187_at	cytochrome P450 2A1	Drug & secondary metabolism	2608	-1.4	-5.4***
M33312cds_s_at	cytochrome P450 2A1	Drug & secondary metabolism	2315	-1.1	-2.1**
U33540exon_f_at	cytochrome P450 2B3	Drug & secondary metabolism	1463	-1.9	-2.9*
L00320cds_f_at	cytochrome P450 2B19	Drug & secondary metabolism	124	3.5	8**
rc_AA945573_f_at	cytochrome P450 2C7	Drug & secondary metabolism	3541	-1.6**	-5**
J02657_s_at	cytochrome P450 2C11	Drug & secondary metabolism	7305	-1.5**	-4.5**
J02861mRNA_s_a	cytochrome P450 2C13	Drug & secondary metabolism	4840	-1.3	-2.6***
M33550cds_s_at	cytochrome P450 2C40	Drug & secondary metabolism	252	-1.4	4*
J02869mRNA_s_a	cytochrome P450 2D1	Drug & secondary metabolism	6189	-1.6*	-2.2**
AB008424_s_at	cytochrome P450 2D3	Drug & secondary metabolism	3513	-1.3	-3.6**
L24207_r_at	cytochrome P450 3A3	Drug & secondary metabolism	181	1.2	2.3*
U39206_at	cytochrome P450 4F4	Drug & secondary metabolism	628	-1.2	-2.9**
U39208_at	cytochrome P450 4F6	Drug & secondary metabolism	1702	-1.5	-2.2**
U40004_s_at	cytochrome P450 monooxygenase	Drug & secondary metabolism	498	-1.1	-2.4**
AF045464_s_at	aflatoxin B1 aldehyde reductase	Drug & secondary metabolism	1437	2.5*	4.2**
X81395_at	carboxylesterase 1	Drug & secondary metabolism	242	-1.8	-2.3**
AB010635_s_at	carboxylesterase 2 (intestine, liver)	Drug & secondary metabolism	118	2.3	2.8*
L46791_at	carboxylesterase 3	Drug & secondary metabolism	1518	-1.5	-3.1*
J03867_s_at	diaphorase 1	Drug & secondary metabolism	1049	-1.4	-2.5*
M26125_at	epoxide hydrolase 1	Drug & secondary metabolism	3225	1.6	2.9***
M84719_at	flavin containing monooxygenase 1	Drug & secondary metabolism	886	-1.1	-2.7*
rc_AI169695_f_at	hydroxysteroid sulfotransferase subunit, complete cds	Drug & secondary metabolism	609	-1.3	-3.8*
U01344_g_at	N-acetyltransferase 1 (arylamine N-acetyltransferase)	Drug & secondary metabolism	138	-1.3	-2.1*
U89280_at	oxidative 17 beta hydroxysteroid dehydrogenase type 6	Drug & secondary metabolism	1687	-1.5	-3.3*
L22339_g_at	sulfotransferase family 1A, member 2	Drug & secondary metabolism	4381	-1.7**	-5.6***
rc_AI638982_at	sulfotransferase family, cytosolic, 1C, member 2	Drug & secondary metabolism	285	-1.4	-2.5*
rc_AA945589_at	sulfotransferase, hydroxysteroid preferring 2	Drug & secondary metabolism	243	-1.1	-2.8*
D38066exon_s_at	UDP glycosyltransferase 1 family polypeptide A2	Drug & secondary metabolism	8	-1.5	6.8**
D38061exon_s_at	UDP glycosyltransferase 1 family, polypeptide A6	Drug & secondary metabolism	172	1.4	4.1**
D38062exon_s_at	UDP glycosyltransferase 1 family, polypeptide A7	Drug & secondary metabolism	65	1.6	3.6**
AB010466_s_at	liver multidrug resistance-associated protein 6	Drug & secondary metabolism	689	-1.3	-2.7*
M81855_at	P-glycoprotein/multidrug resistance 1	Drug & secondary metabolism	8	30.2	182.6**
L19031_at	solute carrier family 21, member 1	Drug & secondary metabolism	240	-2*	-2.7**
L27651_g_at	solute carrier family 22 , member 7	Drug & secondary metabolism	954	-1.3	-2.1*
rc_AA800587_at	glutathione peroxidase 2	Stress response	23	2.6	14.5*
rc_AI172411_at	glutathione peroxidase 3	Stress response	255	1.4	2.2**
U73174_g_at	glutathione reductase	Stress response	106	1.3	2.9*
S82820mRNA_s_a	glutathione S-transferase, alpha 1	Stress response	382	4.1**	8.3***
E01415cds_s_at	glutathione S-transferase, mu type 3 (Yb3)	Stress response	567	-1.4	-3.8*
X02904cds_s_at	glutathione S-transferase, pi 2	Stress response	113	3.9*	10.8*
S72506_s_at	glutathione-S-transferase, alpha type2	Stress response	65	4.3**	9.8**
rc_AI170685_at	DnaJ (Hsp40) homolog, subfamily A, member 2	Stress response	290	1.4	2.2**
rc_AA998683_g_a	heat shock 27kDa protein 1	Stress response	143	2.3	7.9**
U68562mRNA#2_s	heat shock protein 60 (liver)	Stress response	408	1.2	3.1**
J02722cds_at	heme oxygenase 1	Stress response	88	2.3	3.9*
rc_AI176456_at	Metallothionein	Stress response	2480	2.9	2.8*
J02679_s_at	NAD(P)H dehydrogenase, quinone 1	Stress response	246	2.3	5.7**
U63923_at	thioredoxin reductase 1	Stress response	420	1.2	2.3*
D85035_g_at	dihydropyrimidine dehydrogenase	Inorganic/cofactor metabolism	440	-1.9*	-3.2**
X99477cds_at	phosphotriesterase related	Inorganic/cofactor metabolism	18	2.3	6.6*
M77479_at	solute carrier family 10, member 1	Inorganic/cofactor metabolism	2433	-1.5*	-5.1***
U75395UTR#1_s_	solute carrier family 12, member 4	Inorganic/cofactor metabolism	43	1.3	3.1*
M97662_at	ureidopropionase, beta	Inorganic/cofactor metabolism	4112	-1.2	-3.3***

[a] Gene expression changes are expressed as a fold change (FC) relative to the mean vehicle signal value, * = $P < 0.05$, ** = $P < 0.01$, *** = $P < 0.001$.

for both transcriptional and intracellular signaling pathways (Figure 1, Table 3). Genes associated with these pathways tended to be associated with cell damage (apoptosis, DNA damage, growth arrest) and repair (cell division). Several transcription factors were also strongly upregulated in the high dose methapyrilene group, including activating transcription factor 3 (ATF3), involved in regulating glucose homeostasis and the stress response.[29]

3.3. Liver Protein Expression Changes. Proteins were compared between the control group and the low dose animals and between the control group and the high dose group. An average of 2860 spots were detected per Cy 3/Cy 5 image pair. After matching and pairwise filtering using the image analysis software's filtering tool, the numbers of protein forms altered between the various experimental groups are given in Table 4. Many protein alterations conserved between the two comparisons were identified by mass spectroscopy, as were several alterations arising from each individual comparison alone. These are summarized in Figure 2 and Table 5 together with the average fold-alterations between the groups. In total, 34 proteins were identified. These comprised 13 conserved elevated proteins and 2 decreased, 4 proteins elevated in the low dose group only, and 5 proteins elevated in the high dose group only with 10 decreased. No proteins were identified that were decreased in the low dose group only. Where a protein was identified as altered over thresholds ($P \leq 0.05$ and fold alteration ≥ 2) in only one group and MS data was available, alteration in the other group was recorded. If altered significantly ($P \leq 0.05$) by any amount, this is recorded also, to complete the data for known proteins. All proteins reported were also significantly altered over all groups by the inbuilt ANOVA test to $P < 0.01$.

In several cases, up-regulation of one form of a protein and down-regulation of other forms of the same protein occurred.

Table 3. Representative Gene Expression Changes Associated with Apoptosis, Cell Division, Transcription, Structural Function, Intracellular Signaling, and Immune Response[a]

Probeset	Gene Title	Pathway	Vehicle Signal value	Methap 50mkd FC	Methap 150mkd FC
D42137exon_s_at	annexin 5	Cell division/apopotosis	269	1.1	2.1*
S76511_s_at	Bcl2-associated X protein	Cell division/apopotosis	27	3.2	7.8**
AJ006971_g_at	Death-associated like kinase	Cell division/apopotosis	216	1.8	2.3**
rc_AI639488_at	mdm2 gene product (LOC314856), mRNA	Cell division/apopotosis	98	2.1	5.7*
rc_AA874794_g_a	nerve growth factor receptor associated protein 1	Cell division/apopotosis	106	1.3	3.8*
M80601_at	programmed cell death 2	Cell division/apopotosis	93	2.1	2.4*
X70871_at	cyclin G1	Cell division/apopotosis	134	2.6	6.8***
rc_AI639082_s_at	mini chromosome maintenance deficient 6 (S. cerevisiae)	Cell division/apopotosis	65	1.1	2.7*
M24604_at	proliferating cell nuclear antigen	Cell division/apopotosis	265	1.1	2.5**
rc_AI180396_at	retinoblastoma-like 2	Cell division/apopotosis	19	1.4	2.2*
rc_AI228599_at	topoisomerase (DNA) 2 alpha	Cell division/apopotosis	130	1.6	2.2*
M76704_s_at	0-6-methylguanine-DNA methyltransferase	Cell division/apopotosis	275	1.4	2.4**
L32591mRNA_at	growth arrest and DNA-damage-inducible 45 alpha	Cell division/apopotosis	117	2.5	5.8**
AF020618_g_at	myeloid differentiation primary response gene 116	Cell division/apopotosis	82	3.1	6.7*
AF087037_at	B-cell translocation gene 3	Cell division/apopotosis	22	3.4*	6.5***
rc_AA944156_s_at	B-cell translocation gene 2, anti-proliferative	Cell division/apopotosis	312	2.6**	4.7
U77829mRNA_s_a	growth arrest specific 5	Cell division/apopotosis	13	4	9.1*
M63282_at	activating transcription factor 3	Transcription/RNA metabolism	51	4	9.9*
rc_AA945867_at	v-jun sarcoma virus 17 oncogene homolog (avian)	Transcription/RNA metabolism	24	3.3*	5.1*
U30186_at	DNA-damage inducible transcript 3	Transcription/RNA metabolism	35	6.7	20.5**
AF023087_s_at	early growth response 1	Transcription/RNA metabolism	329	1.6	4.1*
rc_AI014163_at	interferon-related developmental regulator 1	Transcription/RNA metabolism	88	3.2*	9.6**
L13039_s_at	calpactin I heavy chain	Motility/structural	169	1.4	8.3*
S76054_s_at	keratin complex 2, basic, gene 8	Motility/structural	537	1.8	4.4*
M60666_s_at	tropomyosin 1, alpha	Motility/structural	245	2.8	5.8**
X67788_at	villin 2	Motility/structural	30	2.1	5.1**
J03627_at	S-100 related protein, clone 42C	Intracellular signalling	53	2.7	10.4*
AJ001044cds_at	tumor-associated calcium signal transducer 1	Intracellular signalling	67	1.2	3.5**
X78603_at	ADP-ribosylation factor related protein 1	Intracellular signalling	56	1.2	3.8*
U03390_at	guanine nucleotide binding protein, beta polypeptide 2-like 1	Intracellular signalling	932	1.8	3.6***
rc_AA800291_at	guanylate kinase (LOC303179), mRNA	Intracellular signalling	39	1.8	3.3**
U39572_s_at	phosphatidylinositol 4-kinase	Intracellular signalling	43	1.3	3.1*
L04485mRNA_s_a	mitogen activated protein kinase kinase 1	Intracellular signalling	209	2.1	3.7*
rc_H31287_g_at	NIP kinase	Intracellular signalling	74	16	21.5***
rc_AI178135_at	complement component 1, q subcomponent binding protein	Immune response	214	2.4	3.3**
U20194_at	complement component 8, beta polypeptide	Immune response	999	-2.9*	-3.5**
D10587_g_at	CD36 antigen (collagen type I receptor, thrombospondin recep	Immune response	125	1.8	5.4***
X13044_at	CD74 antigen (invariant polypeptide of major histocompatibili	Immune response	376	1.8*	3.4*
U65217_i_at	RT1 class II, locus Bb	Immune response	61	1.4	4.5**
M22993cds_s_at	alpha(1)-inhibitor 3, variant I	Immune response	2241	-2.4	-3.4**
U44845_at	vitronectin	Immune response	9585	-1.4*	-3.1***

[a] Gene expression changes are expressed as a fold change (FC) relative to the mean vehicle signal value, * = $P < 0.05$, ** = $P < 0.01$, *** = $P < 0.001$.

Table 4. Proteins Altered between Control and Methapyrilene Dosed Groups[a]

dose (mg/kg)	alteration vs control	no. of alterations
50 (low)	elevated	39
50 (low)	decreased	30
150 (high)	elevated	38
150 (high)	decreased	144
both	elevated	18
both	decreased	16

[a] Pairwise comparisons between control and dose groups were carried out using Progenesis V 2004 and spots counted were altered ≥2-fold and with a t-test value of ≤0.05 between groups. The number of spots altered in both groups in each direction is noted in the table.

This is notably the case for carbamoyl phosphate synthase and pyruvate carboxylase. Both are mitochondrial proteins that appear to have been modified by the introduction of a negatively charged group (based on their shift to a more acidic position of similar mass on the gels).

3.4. Liver ^{1}H NMR MAS Metabolic Profile. A visual comparison of the average normalized spectrum for each treatment group readily identifies spectral regions that varied between treatment groups (Figure 3). There were clear, dose-related, changes in both the amounts and composition of fatty acyl species with large changes both to the magnitude and the shapes of the fatty acid methylene and methyl peaks. These broad peaks are comprised of the sum of individual signals for many different fatty acyl species. Furthermore, the high dose animals also showed elevated levels of saturated fatty acyl species by ^{1}H MAS NMR. This can be seen in the elevations of unsaturated ($CH{=}CHCH_2$) and polyunsaturated species ($={CH-CH_2-CH}=$). Trimethylamine N oxide (TMAO) was also elevated in livers of high dose animals. In contrast to lipid and TMAO concentrations both glucose and glycogen levels were depleted slightly in livers of the 50 mg/kg and significantly in the 150 mg/kg dose groups compared to controls.

3.5. Urine Metabolic Profiles. Visual inspection of the ^{1}H NMR spectra from the urine samples did not immediately reveal obvious changes related to the treatments suggesting that consequences of methapyrilene hepatotoxicity were subtle. Initial PCA modeling did not achieve any differentiation of urine samples based on dose due to the subtle nature of the methapyrilene-induced changes. The data were thus subsequently interrogated using orthogonal projections to latent structures discriminant analysis (OPLS-DA). Figure 4 shows the cross-validated scores for the two components of the OPLS-DA model correlated with treatment class. The animals treated with a high dose of methapyrilene were clearly distinct from the low dose and control animals with the day two and day three time points showing the greatest separation from the low dose and control observations suggesting a progression of response to the toxin with time. The high dose group showed large within group variation.

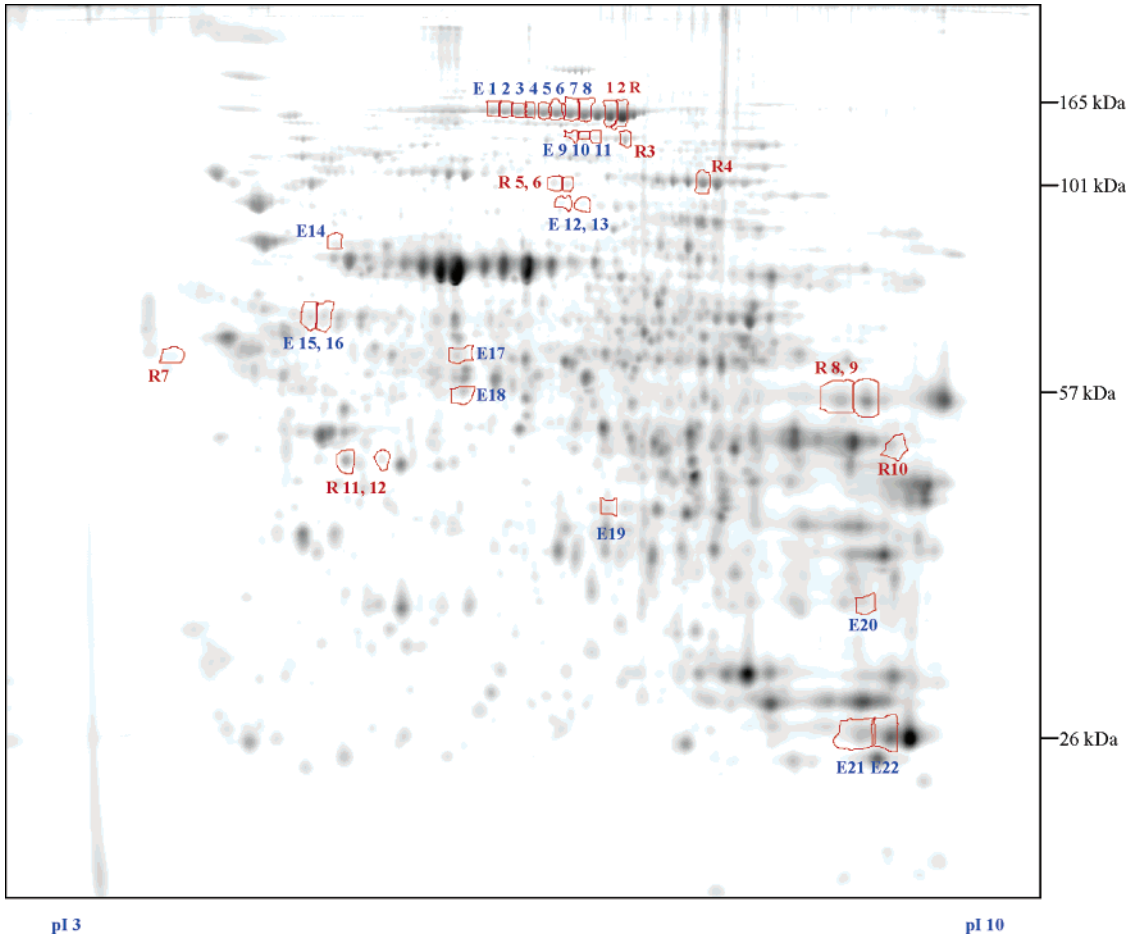

Figure 2. Proteins altered and identified between control and methapyrilene dosed groups. Proteins are numbered *E'x'* where elevated and *R'x'* where reduced. The spot number refers to the reference gel spot number.

The variable coefficients from the OPLS model indicate which of the regions of the spectrum, and hence metabolites, are predominantly responsible for distinguishing the high dose from control and low dose urine samples (Figure 5). High dose animals excreted higher quantities of 1-methylnicotinamide, adipate, succinate and dimethylglycine compared to control and low dose animals. In comparison with urine samples from control animals, those obtained from the low dose group manifested higher urinary levels of succinate and dimethylglycine.

4. Discussion

Mammalian systems have a degree of complexity far above that of simple eukaryotes and prokaryotes which has precluded the widespread application of formalized "bottom up" modeling approaches such as metabolic flux balancing. Considerable work is therefore needed to incorporate contributions from the additional complications such as inter-compartmental communication as well as influences of symbionts and broader physiological processes to turn current black box models into working mathematical descriptions of biological systems. This in itself will require biologically meaningful and well-characterized data sets representing mammalian organisms at a systems level such as we present here.

The combination of information from gene, protein and metabolite levels provides an integrated picture of the response to methapyrilene-induced hepatotoxicity with mutually supporting and mutually validating evidence arising from each biomolecular level. As expected there were several instances where genes and proteins, either encoded by the same gene or by other genes within the same pathway, were both co regulated by methapyrilene toxicity, and sometimes this was in concert with an associated metabolic product (Table 6). This demonstrates the synergy that might be expected from combining these parallel omic approaches. Measurements made across multiple biomolecular levels as used here could potentially yield biomarker combinations that are more specific than combination biomarkers derived from one omic platform alone. Over and above the biological insight this work has highlighted a number of areas that should be of general consideration and require continuous refinement in an approach to systems biology utilizing parallel omic technologies.

The first area concerns the strategy of parallel omic data sets. It should be noted that alterations in expression of genes or enzyme levels and modification of protein forms, while suggesting a potential target of toxic effects, do not imply that function or activity must be altered. This means that from gene and proteomic expression profiling alone, the distinction between causative effects and simple 'read-out' of a more general effect is not possible. Alterations to metabolic profiles reflect function and so may serve to aid interpretation of corresponding gene expression and proteomic analyses. In this respect, the metabolic profile is indicative of functional status with the corresponding gene and protein expression measures

Table 5. Proteins Altered by High and Low Dose Methapyrilene Treatment and Identified by MS[a]

spot (Figure 5)	fold alteration in mean vs control by dose		identity	accession
	low	high		
			Elevated	
775 E1	3.9	11.5	Carbamoyl phosphate synthase	CPSM
779 E2	6.7	17.8	Carbamoyl phosphate synthase	CPSM
782 E3	14.2	33.3	Carbamoyl phosphate synthase	CPSM
788 E4	9.1	16.4	Carbamoyl phosphate synthase	CPSM
790 E5	13.5	20.3	Carbamoyl phosphate synthase	CPSM
793 E6	7.1	9.0	Carbamoyl phosphate synthase	CPSM
794 E7	4.0	4.1	Carbamoyl phosphate synthase	CPSM
798 E8	2.2	x	Carbamoyl phosphate synthase	CPSM
953 E9	32.6	66.8	Pyruvate carboxylase	PYC
957 E10	3.6	x	Pyruvate carboxylase	PYC
970 E11	2.2	2.6	Pyruvate carboxylase	PYC
1414 E12	5.1	x	Dimethylglycine dehydrogenase	M2GD
1419 E13	3.2	x	Dimethylglycine dehydrogenase	M2GD
1604 E14	3.7	3.9	Stress-70 protein precursor	GR75
1898 E15	2.1	2.8	Hsp60 precursor	CH60
1899 E16	*1.9*	3.0	Hsp60 precursor	CH60
2036 E17	*1.8*	2.1	Protein disulfide isomerase A3 precursor	PDA3
2164 E18	4.2	3.0	Phenylalanine-4-hydroxylase	PH4H
2454 E19	x	2.5	Ornithine carbamoyltransferase	OTC
2660 E20	2.4	3.0	Short chain 3-hydroxyacyl-CoA dehydrogenase	HCDH
2863 E21	x	2.2	Glutathione-S-Transferase	GTM1
2869 E22	x	2.5	Glutathione-S-Transferase	GTM1
			Reduced	
816 R1	x	−2.4	Carbamoyl phosphate synthase	CPSM
822 R2	x	−3.7	Carbamoyl phosphate synthase	CPSM
992 R3	x	−3.0	Pyruvate carboxylase	PYC
1290 R4	x	−2.0	Elongation factor 2	EF2
1303 R5	−2.0	−3.1	Sarcosine dehydrogenase, mitochondrial precursor	SARH
1311 R6	−2.6	−4.7	Sarcosine dehydrogenase, mitochondrial precursor	SARH
2040 R7	x	−2.4	Calreticulin	CRTC
2183 R8	x	−2.2	Hydroxylmethylglutaryl − Co A synthase	HMCM
2187 R9	x	−3.5	Hydroxylmethylglutaryl − Co A synthase	HMCM
2306 R10	x	−2.9	3-ketoacyl CoA dehydrogenase, mitochondrial	THIM
2333 R11	*−1.6*	−2.7	Fructose 1,6 bisphosphatase	F16P
2338 R12	x	−2.6	Fructose 1,6 bisphosphatase	F16P

[a] All spots are here marked on the reference gel image (derived from the standard Cy 5 channel of gel 4). Proteins are numbered *E'x'* where elevated and *R'x'* where reduced. The spot number refers to the reference gel spot number. Negative values indicate a down-regulation. '*x*' indicates no significant alteration in a dose group against the control. Where a spot altered significantly and by at least 2-fold in only one group (hence meeting thresholds) showed a significant but sub 2-fold alteration in the other group, this is noted in italics. All accessions are 'accession_rat,' from Swiss-Prot, unless otherwise noted.

best interpreted as the homeostatic response to the current metabolic "challenge". In higher eukaryotes the correlation between changes in expression of the genome and the proteome on a gene-by-gene basis can be poor[30] thus modulation of pathways at some or all biomolecular levels could indicate a critical control point. In addition combining the different approaches offers other advantages as proteomics can also indicate changes in protein modification as well as abundance and metabolic changes are likely to be distal to many of signal transduction changes detected by gene expression changes. Furthermore, as metabolites unlike genes do not suffer the problem of orthology, observed metabolic effects are likely to be highly conserved between species and integrated systems approaches applied to two species may be one framework within which to reconcile and understand the similarities and differences in genetic wiring of common biological processes between different species.

A second issue is that of experimental design. Here it may well be the case that looking at time points where toxicity is already well developed mitigates against obtaining a clear understanding of the temporal dynamics of the mechanism, especially as changes at the gene, protein and metabolite level may proceed at different rates and on different time scales. As such we might expect highly non linear relationships between the concentrations of various species at the different levels of biomolecular organization. Analysis of such complex data sets is challenging, and with current tools involves a degree of subjectivity. It may therefore be the case that more subtle relationships present in these data linking the various levels of biomolecular organization within the cell have been missed. More generally this would suggest the importance of a time course where possible in future experimental designs.

The third area might be termed analytical resolution. The DNA microarray method measures the expression of individual genes and a single expression numerical value can be derived for each. The proteomic and metabonomics approaches used here do not yield individual numerical values for every species measured since the response is measured as the overall change in profile where the variables measured are expressed in terms of differential responses or relative changes. This presents a significant modeling challenge and is one reason latent variable methods dominate the metabonomics literature. In this instance, we detected 100s of gene expression changes compared to the relatively small number of changes detected by the other two technologies. It may thus be likely that insufficient detail was obtained at each biomolecular level to elaborate fully on mechanism of methapyrilene toxicity. MS based metabolite profiling methods may uncover further mechanistic informa-

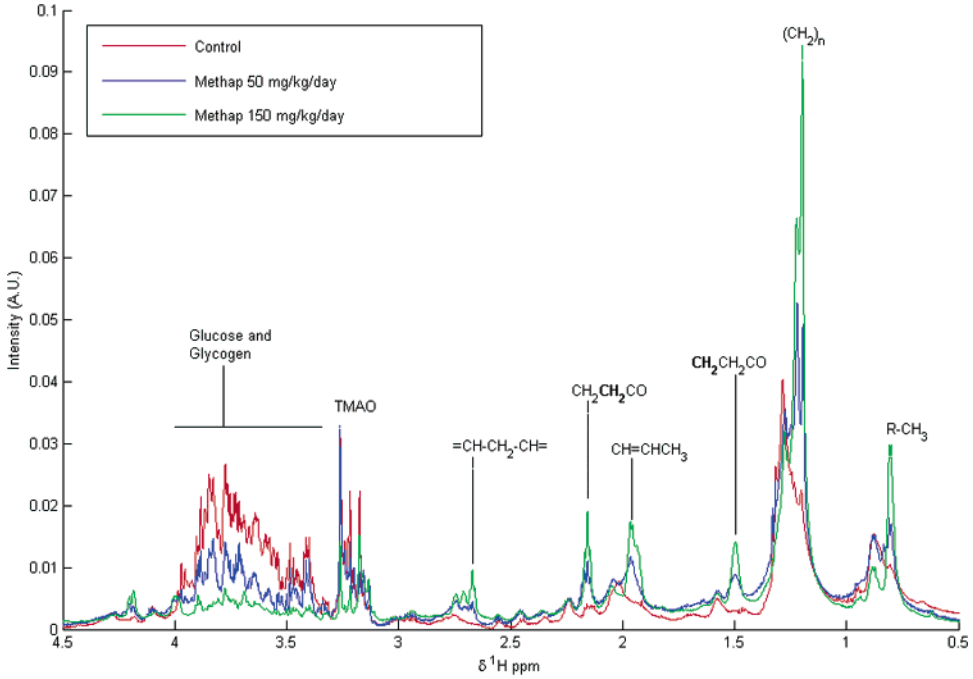

Figure 3. Average standard ^{1}H MAS NMR spectra of liver from each treatment group. This figure shows clearly dose related elevations and composition changes in fatty acid species as indicated by the change in shape of the CH_2 and CH_3 peaks in the regions of 1.3 and 0.9 ppm, respectively. Trimethylamine-*N*-oxide (TMAO) levels are also elevated in high dose animals There is also a clear decrease in liver glucose and glycogen levels.

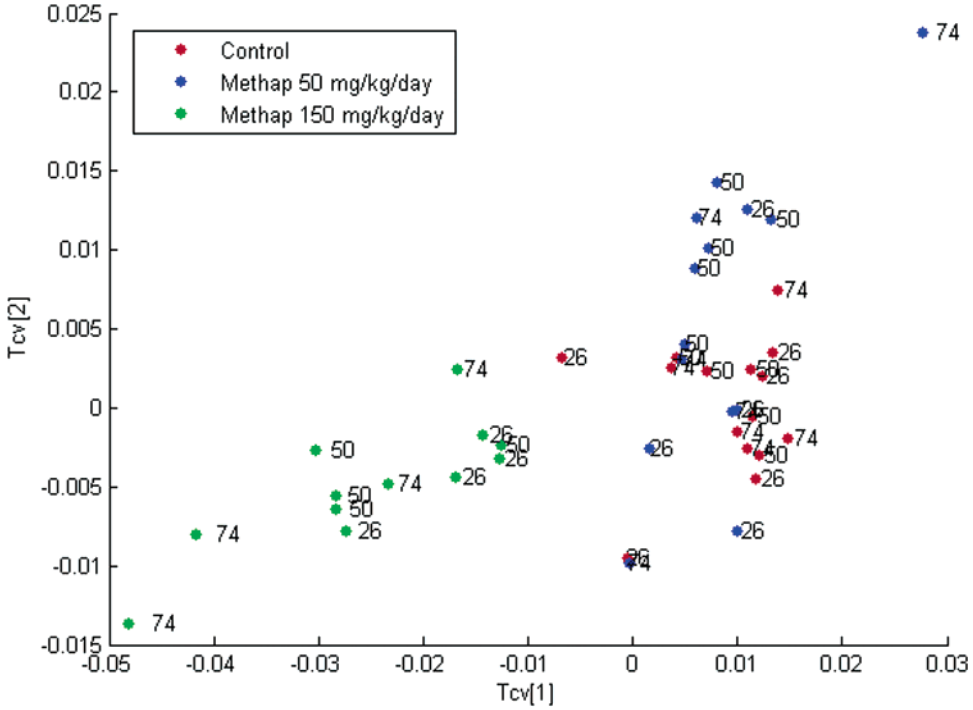

Figure 4. Plot of OPLS DA Tcv[1]/Tcv[2] cross-validated scores derived from ^{1}H NMR spectra of the urine samples, showing some separation of samples according to classification by treatment. The data were mean centered and scaled to unit variance prior to modeling. Key: color code indicates class; red = control; blue = 50 mg/kg; green = 150 mg/kg. Numerical values indicate the time of sampling, for example 26 represents the urine samples collected between 0 and 26 h after dosing.

tion and have been shown to be highly complementary to NMR profiling techniques. However, it may be necessary to await more sensitive metabonomic and proteomic technologies to enable total resolution of signaling and regulatory pathways in addition to the metabolic pathways.

Consideration should also be given to the statistical difficulties in combining 'omics'; data sets or data generated from separate analytical platforms. Since each data type usually requires tailored preprocessing (normalization, transformation, scaling, etc.) combining multiple data sets presents a significant

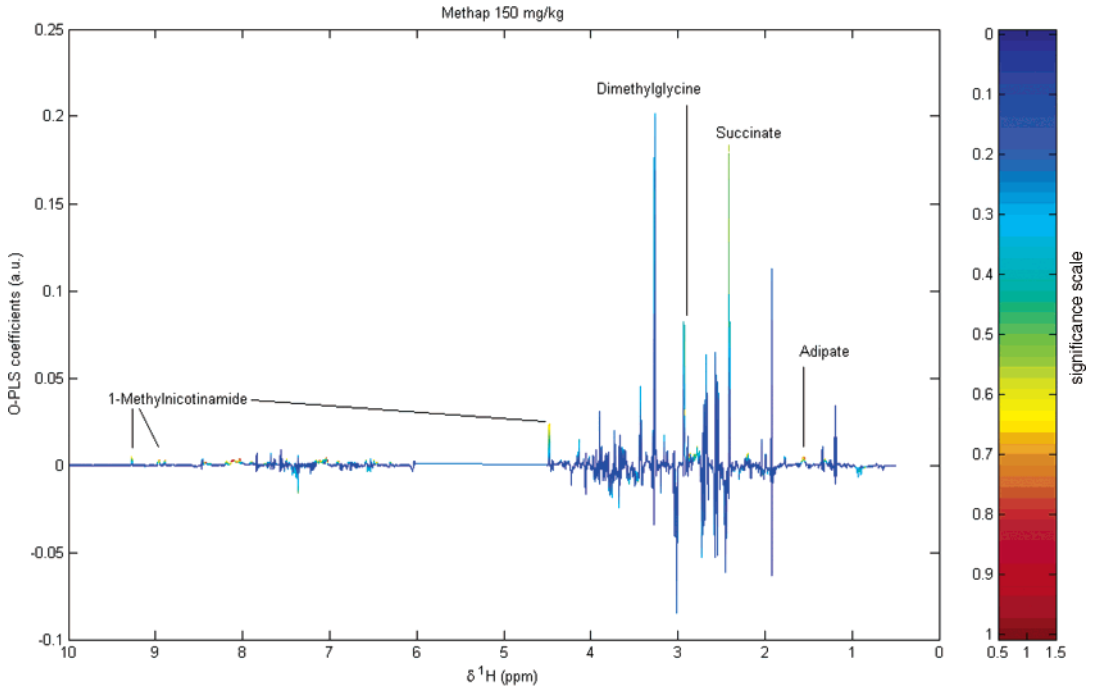

Figure 5. Plot of OPLS DA coefficients describing which spectral regions are diagnostic of high dose (150 mg/kg) methapyrilene intoxication. High dose animals excrete higher levels of 1-methylnicotinamide, adipate, succinate, and dimethylglycine compared to control and low dose animals as indicated by the color of the metabolite signals with respect to the scale of significance.

analytical challenge. Here, we have performed a separate analysis at the gene, protein, and metabolite level and integrated the knowledge gained from each data set to uncover pathways which responded to the methapyrilene-induced toxicity.

3.5. Biological Discussion. The administration of both 50 and 150 mg/kg/day of methapyrilene was associated with changes at the gene, protein, and metabolite level. However, the lower dose resulted in minimal toxicity, and therefore, it may be assumed that the bulk of the changes seen resulted from the pharmacology of the drug. The significant histopathological and serum liver enzyme level changes seen as a result of methapyrilene administration at 150 mg/kg/day were also reflected in changes at the biomolecular level. Thus, the liver gene transcript profiles, protein profiles and metabolite profiles all showed significant, dose related, changes as a consequence of methapyrilene at this dose level. The gene expression changes described in this report after 3 days of methapyrilene administration are consistent with previous studies which have described the application of microarray technology after 24 hours[8] or 7 days[9] with changes observed in the expression of genes associated with stress and apoptosis, and also metabolic pathways for glucose, fatty acids, retinoid and xenobiotics. Although there have been a number of proteomic investigations on methapyrilene hepatotoxicity,[10−12] the identity of the affected proteins is largely unknown. There are no previous reports of global metabolic profiling being applied to this model.

From an examination of the three data sets common biological themes emerge. At each of the levels of gene expression, protein expression and global metabolic profiles dose dependent changes were seen that were related to stress responses and to changes in metabolic pathways involving lipid, glucose and choline metabolism and the urea cycle (Table 6). This approach of grouping individual changes into pathways of action is not a new one but is useful in trying to interpret these large datasets.[31]

3.6. Stress Response. A general stress response was evident, from both the gene expression and proteomic observations. Heat shock protein 60 gene expression and protein level were induced by 150 mg/kg/day methapyrilene. Heat shock protein 60 is a mitochondrial chaperone protein that was down regulated in acetaminophen (APAP) hepatotoxicity.[32] The expression of heat shock protein 27 and 40 genes was also induced. These chaperone proteins are induced in response to stress in the endoplasmic reticulum and changes in these genes were accompanied by changes in proteins involved in protein folding in this organelle such as stress-70 protein (elevated) calreticulin (reduced), protein disulfide isomerase A3 (elevated).

A number of genes normally associated with the stress response were upregulated and included heme oxygenase 1, metallothionein, and NAD(P)H quinone 1 reductase. A common feature of these genes is that they are up-regulated at the transcriptional level by oxidative damage by the transcription factor Nrf-2.[33] The glutathione system is part of the cellular defense against oxidative damage, and this was evident by increased gene expression of several members of the glutathione *S*-transferase and glutathione peroxidase families. Glutathione *S*-transferase was also increased at the protein level. However although these observations are indicative of oxidative damage, it is important to note that no changes were found for glutathione *S*-transferase activity or cytostolic glutathione in a comparable study with methapyrilene dosed rats.[17] Additional responses to tissue damage were revealed by gene expression, with alterations in apoptotic and cell division pathways consisting of entirely upregulated genes (Figure 1).

3.7. Fuel Metabolism. Liver glucose and glycogen levels detected by ^{1}H MAS NMR were significantly depleted by methapyrilene at 150 mg/kg/day, and to a lesser extent by the 50 mg/kg dose, and this was accompanied by a general decrease in the level of genes and proteins associated with carbohydrate metabolism (Table 6). This suggests that hepatic

Table 6. Common Gene, Protein, and Metabolite Changes Associated with Methapyrilene Toxicity[a]

pathway	gene	protein	metabolite
Stress	Heat shock protein 60 ↑	Heat shock protein 60 ↑	
	Glutathione s-transferase alpha 1 ↑	Glutathione-S− transferase ↑	
	DnaJ (hsp40) homolog, A2 ↑		
	Heat shock 27kda protein 1 ↑		
	NAD(P)H quinone dehydrogenase ↑		
	Thioredoxin reductase 1 ↑		
	Heme oxygenase 1 ↑		
	Metallothionein ↑		
		Stress-70 protein precursor ↑	
		Protein disulfide isomerase A3 ↑	
		Calreticulin	
Glucose metabolism	Fructose-1,6 bisphosphatase 1↓	Fructose 1,6 bisphosphatase↓	Glucose↓
	Pyruvate carboxylase ↓	Pyruvate carboxylase ↓(↑*)	Glycogen ↓
	Pyruvate kinase ↓		
	Aldolase A/B ↓		
	Glucokinase ↓		Succinate (urine) ↑
Lipid metabolism		Mitochondrial HMG-CoA synthase ↓	
		Short chain 3-hydroxyacyl-CoA dehydrogenase ↑	Triglycerides ↑
		3-Ketoacyl CoA dehydrogenase ↓	[Adipate (urine)] ↑
	Mitochondrial Acyl-CoA thioesterase 1 ↑		
	Malic enzyme 1 ↓		
	ATP citrate lyase ↓		
	Fatty acid CoA ligase 1/5 ↓		
	Stearoyl-CoA desaturase 1 ↓		Saturated fatty acids ↑
Urea cycle	Ornithine carbamoyltransferase↑	Ornithine carbamoyltransferase↓	
	Argininosuccinate lyase ↑	Carbamoyl phosphate synthase ↓(↑*)	
	Ornithine decarboxylase 1 ↑		
Choline metabolism	Dimethylglycine dehydrogenase ↓	Dimethylglycine dehydrogenase ↑	Dimethylglycine (urine) ↑
	Glycine methyltransferase ↓		
		Sarcosine dehydrogenase ↑	[TMAO (urine)↑]
Phenyl-alanine metabolism	Phenylalanine 4-hydroxylase ↓	Phenylalanine-4-hydroxylase ↑	

[a] Arrows indicate direction of change, (*) indicates mitochondrial proteins with apparently charged covalent modification. Metabolites changes were identified in liver unless stated otherwise.

glycolysis was potentially increased and gluconeogenesis was decreased. Evidence for the latter is provided by decreased levels of the gluconeogenic enzymes fructose 1,6-bisphospahatase and pyruvate carboxylase, at both gene and protein levels. In addition pyruvate carboxylase is a mitochondrial protein that was apparently modified by introduction of a negatively charged group in the 150 mg/kg/day group.

A number of biomolecular changes suggest that mitochondrial fatty acid β-oxidation was impaired in response to methapyrilene toxicity. The elevated levels of triglycerides in the livers of animals treated with both 50 and 150 mg/kg/day animals detected by ^{1}H MAS NMR must derive from mobile lipid reservoirs within the cell or they would not be visible by NMR spectroscopy due to extremely fast relaxation. Microvesicular lipid droplets have previously been shown to form in response to methapyrilene[8] and would therefore be the most likely candidate pool. Phenylalanine-4-hydroxylase protein was increased in both groups, whereas the gene was down regulated. This enzyme is involved phenylalanine catabolism and is altered in drug-induced microvesicular steatosis in rats and may participate in the formation of acetyl-CoA under conditions of blocked β-oxidation.[34] The mitochondrial form of HMG-CoA synthase was downregulated at the protein level. This enzyme is involved in the synthesis of ketone bodies from acetyl-CoA. Short chain 3-hydroxyacyl-CoA dehydrogenase is part of the β-oxidation pathway that ultimately forms acetyl-CoA, and the protein was increased in both dose groups. Elevated urinary adipate levels were observed in high dose treated animals. Adipate is a product of γ-oxidation of fatty acids and may thus reflect a failure of β-oxidation and a shunt of substrate to this alternative pathway. Elevated urinary adipate excretion has been reported in human peroxisomal disorders.[35]

There were alterations to the composition of both unsaturated and saturated fatty acyl species as determined by ^{1}H MAS NMR, with high dose animals showing higher levels of saturated species. This was reflected by the substantial downregulation of stearoyl-CoA-desaturase genes 1 and 2, which encode the rate-limiting enzyme in the synthesis of monosaturated fatty acids.

3.8. Other Metabolism. There was also evidence of modulation of both the urea cycle and choline metabolism (Table 6). Enzymes with the urea cycle were modulated at either the gene or protein level, although no change in metabolic intermediates was detected. Within the urea cycle, the enzyme carbamoyl phosphate synthase, which is located in the mitochondrial matrix, showed charge modification, which might be explained by e.g., covalent modification. Dimethylglycine is formed during the catabolism of choline, and levels of this metabolite were elevated in urine in response to methapyrilene. Mitochondrial enzymes within this pathway were also altered at the gene and/or protein level, including dimethylglycine dehydro-

genase which catalyses the formation of sarcosine from dimethylglycine, and sarcosine dehydrogenase which converts sarcosine to glycine. Choline is also degraded to trimethylamine by gut bacteria and this is oxidized in the liver to form trimethylamine oxide (TMAO). The appearance of TMAO in the urine of the 150 mg/kg methapyrilene-dosed rats again suggests enhanced choline metabolism. This may be of significance as a choline deficient diet enhances the toxicological effects of methapyrilene.[36]

3.9. Carcinogenesis. Finally the high dose animals excreted more *N*-methylnicotinamide in the urine than the control or low dose group. Unusually this occurred in the absence of changes in associated protein or genes for the nicotinamide pathway. Elevated excretion of this molecule has been proposed as a potential biomarker for peroxisomal proliferation,[37] which is accompanied by induction of number of genes associated with β-oxidation including mitochondrial thioesterase 1.[38] Although methapyrilene is not associated with peroxisome proliferation, strong induction of the thioesterase gene expression was observed. This may simply be a reflection of the inhibition of fatty acid β-oxidation already discussed, or as both methapyrilene and peroxisome proliferators are known rodent nongenotoxic hepatocarcinogens.[12] This may suggest a common mechanism for liver tumor formation.

3.10. Mechanism of Methapyrilene Toxicity. Previous studies have suggested that a metabolite of methapyrilene covalently binds almost exclusively to mitochondrial protein[11,22] and that toxicity results in dislocation of the mitochondrial membranes.[20] In this present study, two mitochondrial proteins (pyruvate carboxylase and carbamoyl phosphate synthase) underwent modification to negatively charged species. This modification is consistent with covalent adduct formation as a result of the generation of a reactive metabolite of the drug however, further studies are required to confirm this hypothesis. With respect to the observed toxicity it is noteworthy that many of the metabolic processes that were apparently affected by methapyrilene (gluconeogenesis, fatty acid β-oxidation, urea cycle choline metabolism) are, in the main, catalyzed by enzymes residing within mitochondria. Mitochondrial dysfunction causes oxidative stress, the hall marks of which were observed in the gene and protein stress response, and eventual cell death either through apoptosis or necrosis.

The alterations described within this report have been seen with other toxins and disorders suggest that such changes are not specific to methapyrilene, which is not surprising given the sharing of many targets between hepatotoxins and is consistent with previous data.[39] For instance similar metabolic and gene expression effects have been observed in studies of acute APAP toxicity in mice.[32,40] APAP induces centrilobular necrosis, an endpoint not entirely equivalent to that of the periportal necrosis due to methapyrilene toxicity. It is not possible to determine if the metabolic changes detected here are directly part of the causal mechanism of the toxicity exhibited by methapyrilene or APAP. However, these common responses suggest that the metabolic changes evidenced here and elsewhere may represent a common disruption to energy metabolism induced by hepatocellular necrotic agents.

Despite the similarities in the biomolecular changes caused by methapyrilene compared to other hepatotoxins, there were changes which may relate specifically to the mechanism of methapyrilene toxicity, or at least to formation of a putative reactive metabolite. Genes encoding enzymes involved in drug metabolism were also regulated by methapyrilene at 150 mg/kg/day, (Table 2). In agreement with previous studies[8,41] most P450 genes were down regulated. This included CYP2C11, which has been implicated in the generation of the toxic metabolite of methapyrilene.[17] However CYP2C11 is only expressed in male rats,[14] whereas methapyrilene hepatotoxicity has been observed in both male and female rats.[20] A better candidate may be CYP2C7, which unlike most CYPs is expressed periportally[42] in the region of the liver lobule associated with methapyrilene-induced hepatocyte necrosis. Significantly, CYP2C7 was downregulated by approximately 7-fold in the 150 mg/kg/day methapyrilene dosed rats. Finally as methapyrilene is glucuronidated and secreted into bile[19] it was interesting to observe strong upregulation of UDP glycosyltransferase 1A7/8 and p-glycoprotein drug transporter genes.

4. Conclusions and Future Perspectives

We have characterized the effects of methapyrilene-induced periportal necrosis in rat liver at multiple levels of biomolecular organization. In several instances, we have observed perturbations that are coordinated across the levels of gene expression, protein, and metabolic levels and which have yielded some insight into the general mechanisms of toxicity particularly the relationship between disruption to energy metabolism and hepatocellular necrosis. Further investigations covering the events occurring at earlier time points may help to elucidate the temporal relationships within the molecular events that unfold as toxicity develops. The nature of the covalent binding to the proteins identified here being modified and the effect of that binding on their activity as well as mitochondrial function as reflected by fuel metabolism represent an obvious target for further investigation. Although the capability for investigating disease and gene-environment interactions at a systems level by generating multiple 'omic' data sets is increasing across academic and Biotech laboratories, the integration of such data is non trivial.[43−45] Here, we have presented a conceptual framework within which to integrate and interpret parallel omic data from different analytical platforms and biomolecular levels. We are currently developing a statistical methodology to integrate and data mine complex parallel omic data sets, however, such development will ultimately require further well-characterized and biologically meaningful data sets such as those presented here.

Acknowledgment. The authors would like to thank Sarah Jones, Steve Rayner and Cassie Eaton for assistance with protein mass spectrometry. We would also like to acknowledge and thank BBSRC and AstraZeneca for their financial support in funding A. Craig.

Supporting Information Available: Rat liver gene expression changes (Supplemental Tables 1 and 2). This material is available free of charge via the Internet at http://pubs.acs.org.

References

(1) Gant, T. W.; Baus, P. R.; Clothier, B.; Riley, J.; Davies, R.; Judah, D. J.; Edwards, R. E.; George, E.; Greaves, P.; Smith, A. G. Gene expression profiles associated with inflammation, fibrosis, and cholestasis in mouse liver after griseofulvin. *EHP Toxicogenomics* **2003**, *111* (1T), 37−43.

(2) Azmi, J.; Griffin, J. L.; Antti, H.; Shore, R. F.; Johansson, E.; Nicholson, J. K.; Holmes, E. Metabolic trajectory characterisation of xenobiotic-induced hepatotoxic lesions using statistical batch processing of NMR data. *Analyst* **2002**, *127* (2), 271−276.

(3) Okabe, H.; Satoh, S.; Kato, T.; Kitahara, O.; Yanagawa, R.; Yamaoka, Y.; Tsunoda, T.; Furukawa, Y.; Nakamura, Y. Genome-wide analysis of gene expression in human hepatocellular carcinomas using cDNA microarray: identification of genes involved in viral carcinogenesis and tumor progression. *Cancer Res.* **2001**, *61* (5), 2129−2137.
(4) Griffin, J. L.; Walker, L. A.; Shore, R. F.; Nicholson, J. K. Metabolic profiling of chronic cadmium exposure in the rat. *Chem. Res. Toxicol.* **2001**, *14* (10), 1428−1434.
(5) Kleno, T. G.; Kiehr, B.; Baunsgaard, D.; Sidelmann, U. G. Combination of 'omics' data to investigate the mechanism(s) of hydrazine-induced hepatotoxicity in rats and to identify potential biomarkers. *Biomarkers* **2004**, *9* (2), 116−138.
(6) Ruepp, S. U.; Tonge, R. P.; Shaw, J.; Wallis, N.; Pognan, F. Genomics and proteomics analysis of acetaminophen toxicity in mouse liver. *Toxicol. Sci.* **2002**, *65* (1), 135−150.
(7) Coen, M.; Ruepp, S. U.; Lindon, J. C.; Nicholson, J. K.; Pognan, F.; Lenz, E. M.; Wilson, I. D. Integrated application of transcriptomics and metabonomics yields new insight into the toxicity due to APAP in the mouse. *J. Pharm. Biomed. Anal.* **2004**, *35* (1), 93−105.
(8) Hamadeh, H. K.; Knight, B. L.; Haugen, A. C.; Sieber, S.; Amin, R. P.; Bushel, P. R.; Stoll, R.; Blanchard, K.; Jayadev, S.; Tennant, R. W.; Cunningham, M. L.; Afshari, C. A.; Paules, R. S. Methapyrilene toxicity: anchorage of pathologic observations to gene expression alterations. *Toxicol. Pathol.* **2002**, *30* (4), 470.
(9) Waring, J. F.; Ulrich, R. G.; Flint, N.; Morfitt, D.; Kalkuhl, A.; Staedtler, F.; Lawton, M.; Beekman, J. M.; Suter, L. Interlaboratory evaluation of rat hepatic gene expression changes induced by methapyrilene. *Environ. Health Perspect.* **2004**, *112* (4), 439.
(10) Anderson, N. L.; Copple, D. C.; Bendele, R. A.; Probst, G. S.; Richardson, F. C. Covalent protein modifications and gene expression changes in rodent liver following administration of methapyrilene: a study using two-dimensional electrophoresis. *Fundam. Appl. Toxicol.* **1992**, *18* (4), 570.
(11) Richardson, F. C.; Strom, S. C.; Copple, D. M.; Bendele, R. A.; Probst, G. S.; Anderson, N. L. Comparisons of protein changes in human and rodent hepatocytes induced by the rat-specific carcinogen, methapyrilene. *Electrophoresis* **1993**, *14* (1−2), 157.
(12) Cunningham, M. L.; Pippin, L. L.; Anderson, N. L.; Wenk, M. L. The hepatocarcinogen methapyrilene but not the analogue pyrilamine induces sustained hepatocellular replication and protein alterations in F344 rats in a 13-week feed study. *Toxicol. Appl. Pharmacol.* **1995**, *131* (2), 216.
(13) Jaeschke, H.; Knight, T. R.; Bajt, M. L. The role of oxidant stress and reactive nitrogen species in acetaminophen hepatotoxicity. *Toxicol. Lett.* **2003**, *144* (3), 279−288.
(14) Oinonen, T.; Lindros, K. O. Zonation of hepatic cytochrome P-450 expression and regulation. *Biochem. J.* **1998**, *329* (Pt 1), 17−35.
(15) Sasse, D.; Maly, I. P. Studies on the periportal hepatotoxicity of allyl alcohol. *Prog. Histochem. Cytochem.* **1991**, *23* (1−4), 146−149.
(16) Graichen, M. E.; Neptun, D. A.; Dent, J. G.; Popp, J. A.; Leonard, T. B. Effects of methapyrilene on rat hepatic xenobiotic metabolizing enzymes and liver morphology. *Fundam. Appl. Toxicol.* **1985**, *5* (1), 165−174.
(17) Ratra, G. S.; Cottrell, S.; Powell, C. J. Effects of induction and inhibition of cytochromes P450 on the hepatotoxicity of methapyrilene. *Toxicol. Sci.* **1998**, *46* (1), 185−196.
(18) Ratra, G. S.; Morgan, W. A.; Mullervy, J.; Powell, C. J.; Wright, M. C. Methapyrilene hepatotoxicity is associated with oxidative stress, mitochondrial disfunction and is prevented by the Ca2+ channel blocker verapamil. *Toxicology* **1998**, *130* (2−3), 79.
(19) Ratra, G. S.; Powell, C. J.; Park, B. K.; Maggs, J. L.; Cottrell, S. Methapyrilene hepatotoxicity is associated with increased hepatic glutathione, the formation of glucuronide conjugates, and enterohepatic recirculation. *Chem. Biol. Interact.* **2000**, *129* (3), 279−295.
(20) Reznik-Schuller, H. M.; Lijinsky, W. Ultrastructural changes in the liver of animals treated with methapyrilene and some analogues. *Ecotoxicol. Environ. Saf.* **1982**, *6* (4), 328−335.
(21) Richardson, F. C.; Horn, D. M.; Anderson, N. L. Dose−responses in rat hepatic protein modification and expression following exposure to the rat hepatocarcinogen methapyrilene. *Carcinogenesis* **1994**, *15* (2), 325−329.
(22) Reznik-Schuller, H. M.; Lijinsky, W. Morphology of early changes in liver carcinogenesis induced by methapyrilene. *Arch Toxicol.* **1981**, *49* (1), 79−83.
(23) Tonge, R.; Shaw, J.; Middleton, B.; Rowlinson, R.; Rayner, S.; Young, J.; Pognan, F.; Hawkins, E.; Currie, I.; Davison, M. Validation and development of fluorescence two-dimensional differential gel electrophoresis proteomics technology. *Proteomics* **2001**, *1* (3), 377−396.
(24) Neuhoff, V.; Stamm, R.; Eibl, H. Clear background and highly sensitive protein staining with Coomassie Blue dyes in polyacrylamide gels: A systematic analysis. *Electrophoresis* **1985**, *6*, 427.
(25) Blum, H.; Beier, H.; Gross, H. J. Improved silver staining of plant proteins, RNA, and DNA in polyacrylamide gels. *Electrophoresis* **1987**, *8*, 93.
(26) Neuhoff, V.; Arold, N.; Taube, D.; Ehrhardt, W. Improved staining of proteins in polyacrylamide gels including isoelectric focusing gels with clear background at nanogram sensitivity using Coomassie Brilliant Blue G-250 and R-250. *Electrophoresis* **1988**, *9*, 255.
(27) Trygg, J.; Wold, S., O2−PLS, a two-block (X−Y) latent variable regression (LVR) method with an integral OSC filter. *J. Chemomet.* **2003**, *17* (1), 53−64.
(28) Cloarec, O.; Dumas, M. E.; Trygg, J.; Craig, A.; Barton, R. H.; Lindon, J. C.; Nicholson, J. K.; Holmes, E. Evaluation of the orthogonal projection on latent structure model limitations caused by chemical shift variability and improved visualization of biomarker changes in 1HNMR spectroscopic metabonomic studies. *Anal. Chem.* **2005**, *77* (2), 517−526.
(29) Allen-Jennings, A. E.; Hartman, M. G.; Kociba, G. J.; Hai, T. The roles of ATF3 in glucose homeostasis. A transgenic mouse model with liver dysfunction and defects in endocrine pancreas. *J. Biol. Chem.* **2001**, *276* (31), 29507−29514.
(30) Prabhakar, U.; Conway, T. M.; Murdock, P.; Mooney, J. L.; Clark, S.; Hedge, P.; Bond, B. C.; Jazwinska, E. C.; Barnes, M. R.; Tobin, F.; Damian-Iordachi, V.; Greller, L.; Hurle, M.; Stubbs, A. P.; Li, Z.; Valoret, E. I.; Erickson-Miller, C.; Cass, L.; Levitt, B.; Davis, H. M.; Jorkasky, D. K.; Williams, W. V. Correlation of protein and gene expression profiles of inflammatory proteins after endotoxin challenge in human subjects. *DNA Cell Biol.* **2005**, *24* (7), 410−431.
(31) Lin, B.; White, J. T.; Lu, W.; Xie, T.; Utleg, A. G.; Yan, X.; Yi, E. C.; Shannon, P.; Khrebtukova, I.; Lange, P. H.; Goodlett, D. R.; Zhou, D.; Vasicek, T. J.; Hood, L. Evidence for the presence of disease-perturbed networks in prostate cancer cells by genomic and proteomic analyses: a systems approach to disease. *Cancer Res.* **2005**, *65* (8), 3081−3091.
(32) Ruepp, S. U.; Tonge, R. P.; Shaw, J.; Wallis, N.; Pognan, F. Genomics and Proteomics Analysis of Acetaminophen Toxicity in Mouse Liver. *Toxicol. Sci.* **2002**, *65* (1), 135−150.
(33) Nguyen, T.; Yang, C. S.; Pickett, C. B., The pathways and molecular mechanisms regulating Nrf2 activation in response to chemical stress. *Free Radic. Biol. Med.* **2004**, *37*, (4), 433−41.
(34) Meneses-Lorente, G.; Guest, P. C.; Lawrence, J.; Muniappa, N.; Knowles, M. R.; Skynner, H. A.; Salim, K.; Cristea, I.; Mortishire-Smith, R.; Gaskell, S. J.; Watt, A. A proteomic investigation of drug-induced steatosis in rat liver. *Chem. Res. Toxicol.* **2004**, *17* (5), 605.
(35) Yamaguchi, S.; Iga, M.; Kimura, M.; Suzuki, Y.; Shimozawa, N.; Fukao, T.; Kondo, N.; Tazawa, Y.; Orii, T. Urinary organic acids in peroxisomal disorders: a simple screening method. *J. Chromatogr. B Biomed. Sci. Appl.* **2001**, *758* (1), 81−86.
(36) Perera, M. I.; Katyal, S. L.; Shinozuka, H. Choline deficient diet enhances the initiating and promoting effects of methapyrilene hydrochloride in rat liver as assayed by the induction of gamma-glutamyltranspeptidase-positive hepatocyte foci. *Br. J. Cancer* **1987**, *56* (6), 774−778.
(37) Ringeissen, S.; Connor, S. C.; Brown, H. R.; Sweatman, B. C.; Hodson, M. P.; Kenny, S. P.; Haworth, R. I.; McGill, P.; Price, M. A.; Aylott, M. C.; Nunez, D. J.; Haselden, J. N.; Waterfield, C. J. Potential urinary and plasma biomarkers of peroxisome proliferation in the rat: identification of *N*-methylnicotinamide and *N*-methyl-4-pyridone-3-carboxamide by 1H nuclear magnetic resonance and high performance liquid chromatography. *Biomarkers* **2003**, *8* (3−4), 240−271.
(38) Lanni, A.; Mancini, F.; Sabatino, L.; Silvestri, E.; Franco, R.; De Rosa, G.; Goglia, F.; Colantuoni, V. De novo expression of uncoupling protein 3 is associated to enhanced mitochondrial thioesterase-1 expression and fatty acid metabolism in liver of fenofibrate-treated rats. *FEBS Lett.* **2002**, *525* (1−3), 7−12.
(39) Kim, J.-S.; He, L.; Lemasters, J. J. Mitochondrial permeability transition: a common pathway to necrosis and apoptosis. *Biochem. Biophys. Res. Commun.* **2003**, *304* (3), 463−470.

(40) Coen, M.; Lenz, E. M.; Nicholson, J. K.; Wilson, I. D.; Pognan, F.; Lindon, J. C. An integrated metabonomic investigation of acetaminophen toxicity in the mouse using NMR spectroscopy. *Chem. Res. Toxicol.* **2003**, *16* (3), 295−303.
(41) Waring, J. F.; Ciurlionis, R.; Jolly, R. A.; Heindel, M.; Ulrich, R. G. Microarray analysis of hepatotoxins in vitro reveals a correlation between gene expression profiles and mechanisms of toxicity. *Toxicol. Lett.* **2001**, *120* (1−3), 359−368.
(42) Oinonen, T.; Ronis, M.; Wigell, T.; Tohmo, K.; Badger, T.; Lindros, K. O. Growth hormone-regulated periportal expression of CYP2C7 in rat liver. *Biochem. Pharmacol.* **2000**, *59* (5), 583−589.
(43) Corella, D.; Ordovas, J. M. Integration of environment and disease into omics analysis. *Curr. Opin. Mol. Ther.* **2005**, *7* (6), 569−576.
(44) Thongboonkerd, V. Genomics, proteomics and integrative omics in hypertension research. *Curr. Opin. Nephrol. Hypertens.* **2005**, *14* (2), 133−139.
(45) Zeisel, S H.; Freake, H C.; Bauman, D. E. Bier, D. M.; Burrin, D. G.; German, J. B.; Klein, S.; Marquis, G. S.; Milner, J. A.; Pelto, G. H.; Rasmussen, K. M. The nutritional phenotype in the age of metabolomics. *J. Nutr.* **2005**, *135* (7), 1613−1616.

PR0503376